Preparation, Characterization, and Antimicrobial Activities of ZnO Nanoparticles/Cellulose Nanocrystal Nanocomposites

Susan Azizi,* Mansor Ahmad, Mahnaz Mahdavi, and Sanaz Abdolmohammadi

Zinc oxide (ZnO) nanoparticles were synthesized within cellulose nanocrystals (CNC) as a new stabilizer by a precipitation method for antimicrobial applications. For fabrication of ZnO/CNC nanocomposites, solutions with different molar ratios of Zn to CNC were prepared in ethanol as the solvent. ZnO/CNC was separated from the suspension and then dried at 120 °C for 1 hour. The nanocomposites were characterized using Fourier transform infrared (FTIR), ultraviolet-visible (UV-vis), X-ray diffraction (XRD), transmission electron microscope (TEM), and thermogravimetric (TG) analyses. According to the XRD and TEM results, the ZnO nanoparticles with a hexagonal wurtzite structure were easily prepared and dispersed in the CNC with an average size of less than 20 nm. The average size of the ZnO nanoparticles increased with increasing molar ratio of ZnO to CNC. The best ratio of Zn:CNC was chosen based on the small size of the ZnO nanoparticles that yielded better antimicrobial and thermal properties. The UV-vis absorption spectra of the ZnO/CNC nanocomposites showed absorption peaks in the UV region that were ascribed to the band gap of the ZnO nanoparticles. The antibacterial effects of ZnO/CNC were stronger compared to ZnO nanoparticles.

Keywords: Zinc oxide; Nanocomposite; Cellulose nanocrystal; Antibacterial

*Contact information: Department of Chemistry, Faculty of Science, Universiti Putra Malaysia, 43400 UPM Serdang, Selangor, Malaysia; *Corresponding author: azisusan@gmail.com*

INTRODUCTION

Nano-sized ZnO is a direct wide-band-gap semiconductor with a large exciton binding energy of 60 eV. Due to a variety of attractive physical and chemical properties, it is a promising candidate for a range of applications, such as solar cells (Galoppini *et al.* 2006), gas sensors (Zhang *et al*. 2006), lasing diodes (Huang *et al.* 2001), catalysts (Height *et al.* 2006), and antibacterial agents (Amornpitoksuk *et al.* 2011). It is an effective bactericide against both Gram-positive and Gram-negative bacteria (Tam *et al.* 2008; Zhang *et al.* 2008). Zinc oxide nanoparticles have been reported to disrupt membrane architecture, to change permeability, and to subsequently accumulate in the cytoplasm of bacteria (Stoimenov *et al.* 2002).

Zinc oxide nanoparticles tend to aggregate, owing to a large surface area and high surface energy (Hong *et al.* 2009). For applied systems, the homogenous dispersion of nanoparticles in the different matrices is necessary. In order to prevent nanoparticle aggregation and improve dispersion, a number of novel synthetic approaches have been developed. Recently, the fabrication of inorganic nanoparticles in nanofibular materials has merited substantial attention because of their significant potential applications in the fields of catalysts, electronic nanodevices, optoelectronics, sensors, and nanocomposites

(Liu *et al.* 2010; Yin *et al.* 2010). The physical size of the host polymer and the embedded particles of the composite are both in the submicrometer or nanometer range, so that the typical large surface area of nanofiber materials and nanoparticles is maintained (Patel *et al.* 2007). Furthermore, these nanocomposites have been proven to have both the advantages of polymers (such as being lightweight, flexible, and moldable) and of inorganic particles (such as special functionality, high strength, and thermal stability) (Liu *et al.* 2010; Chronakis 2005; Wang *et al.* 2005).

Cellulose nanocrystals are characteristically rod-formed monocrystals, 1 to 100 nm in diameter and from tens to hundreds of nanometers in length, and produced by controlled acid hydrolysis of cellulose from various sources. Nano-sized cellulose shows such outstanding properties as large aspect ratio (De Souza Lima *et al.* 2003), good dissolvability in water (Shin *et al.* 2008), good mechanical properties (Sturcova *et al.* 2005), minimal thermal degradation behavior (Nishino *et al.* 2004), and a high capacity for absorption of metallic particles (He *et al.* 2003). They can be used in bioenergy, and in chemical, catalytic, and biomedical applications (Liu *et al.* 2011). In most studies, CNC has been applied as a reinforcing phase to improve chemical and physical properties of matrices. Recently, cellulose nanocrystals have been used as a substrate to fabricate nano-sized metallic particles (Cai *et al.* 2009). For example, Au nanoparticles with narrow size distribution were synthesized in cellulose nanocrystals (Khaled *et al.* 2009). In other studies carboxylated cellulose nanocrystals have been used to achieve of metal-containing composites. For example, Ag and Ag–Pd alloy particles with small sizes were separately prepared and dispersed well in carboxylated cellulose nanocrystals (Liu *et al.* 2010). In a suspension of cellulose nanocrystals and metallic salts, most of the metallic particles can adsorb on the surface of CNC due to electrostatic interactions between oxygen atoms of polar hydroxyl and metallic particles (He *et al.* 2003). This effect controls the sizes of metallic nanoparticles by preventing particle agglomeration.

In the present study, ZnO nanoparticles were synthesized within CNC in order to prevent the formation of aggregated ZnO nanoparticles and improve the stability of nanoparticle dispersion. The size, morphology, thermal, optical properties, and antibacterial activity of the resulting ZnO/CNC nanocomposites were studied.

EXPERIMENTAL

Materials

All the reagents were analytical grade and used as received without further purification. Cotton cellulose from filter paper (Q1, Whatman) was provided by Fisher Scientific (Pittsburgh, PA). Sulfuric acid (95-98%, reagent grade) was purchased from Scharlau. Ethanol and sodium hydroxide were supplied from Sigma Aldrich. Zinc acetate dehydrate (99%), used as precursor, was provided by Merck (Germany). All the solutions were prepared with deionized water.

Preparation of Cellulose Nanocrystals

Preparation of the CNC was carried out according to a previous study (Beck-Candanedo *et al.* 2005). The cellulose powder harvested from one filter paper (2 g) was hydrolyzed with a sulfuric acid solution (20 mL, 64 w/w%) at 45 °C for 60 min. The

resultant suspension was diluted 10-fold with cold water (4 °C) followed by centrifuging and dialysis until a neutral pH was reached. Finally, the sample was freeze-dried.

Preparation of ZnO nanoparticles/cellulose nanocrystals nanocomposites

In a typical procedure, zinc oxide cellulose nanocrystals were synthesized by first suspending the CNC in deionized water, then mixing with zinc acetate dehydrate ($Zn(AC)_2$ $2H_2O$) in ethanol by magnetic stirring. The weight ratios of ($Zn(AC)_2$ $2H_2O$):CNC were 2:4, 4:4, and 6:4 (samples 1, 2, and 3, respectively). After complete mixing, a sodium hydroxide solution (5 mol/L) was added drop-wise to the mixed solutions with gentle stirring at 80 °C. The ZnO/CNC nanocomposites were separated into different phases from the suspension by centrifugation and were then washed using distilled water to remove the by-products and extra CNC. After complete washing, the samples were dried at 120 °C for 1 h for complete transformation of the remaining zinc hydroxide to zinc oxide.

Testing for antibacterial activity

The samples were evaluated for antibacterial activity against Gram-negative *Salmonella choleraesuis* and Gram-positive *Staphylococcus aureus*. Six paper discs with a diameter of 6 mm, containing 5 μL of the ZnO/CNC suspensions were placed onto an agar plate that was inoculated with bacteria. Ampicillin and Streptomycin were used as standard antibacterial agents for negative and positive inhibitory controls, respectively. The bacterial inoculum was standardized to 0.5 MF units, which meant that approximately 10^8 colony-forming units of each bacterium were inoculated on a plate. The plates were inverted and incubated at 37 °C for 24 h, then the zone of complete inhibition (including the diameter of the disc) was measured to the nearest whole millimeter, using sliding calipers or a ruler held on the back of the inverted petri plate. Three replicate tests were carried out in the same conditions for each sample. Furthermore, an assay for ZnO nanoparticles with particle size of 20 nm without CNC was also carried out to show the advantage of using ZnO/CNC nanocomposites.

Characterization

Wide-angle X-ray diffraction (WXRD) patterns of the ZnO/CNC and the CNC were recorded using an XPERT-PRO diffractometer at 40 kV and 30 mA from 10° to 80° with nickel-filtered Cu (λ = 1.542 A°) at room temperature. The observed X-ray patterns were compared to the Joint Committee on Powder Diffraction Standards (JCPDS) X-ray data file. The size and morphology of the ZnO/CNC were observed using a Hitachi H-700 transmission electron microscope with an acceleration voltage of 120 kV at room temperature. The TEM sample was prepared by dropping the sample suspension on a Cu grid coated with carbon films, and then the specimens were negatively stained with 1% uranyl acetate and allowed to dry at room temperature. The thermal behavior of the ZnO/CNC powders was recorded with a thermogravimetric analyzer TGA7 (Perkin-Elmer) in a nitrogen atmosphere at a heating rate of 10 °C/min from 25 to 600 °C. The FTIR spectra of the samples were obtained at ambient temperature using the KBr disk method. The disk containing 1 mg of the sample was scanned within a wave number range of 400 to 4000 cm^{-1}. The UV-visible spectra of the ZnO/CNC composites were recorded over the range of 200 to 800 nm with a Lambda 25-Perkin Elmer UV-vis spectrophotometer.

RESULTS AND DISCUSSION

CNC has a high capacity to absorb metallic cations due to abundant hydroxyl groups in its structure. At the first stage of the reaction, Zn^{2+} absorbed via electrostatic interactions between oxygen atoms of hydroxyl and zinc cations. After adding NaOH, $Zn(OH)_2$ was slowly formed. Under thermal condition, ZnO was generated, as was shown by following reactions:

$$Zn^{2+} + CNC \rightarrow Zn^{2+}\ldots CNC \quad (1)$$

$$Zn^{2+} \ldots CNC + 2(OH)^{-} \rightarrow CNC \ldots Zn(OH)_2 \quad (2)$$

$$CNC \ldots Zn(OH)_2 \rightarrow CNC \ldots ZnO + H_2O \quad (3)$$

Characterization of ZnO/CNC

Figure 1 shows the FTIR spectra of the ZnO/CNC nanocomposites. Broad bands in the region of 430 to 442 cm^{-1} can be seen for each spectrum; this is related to the stretch bands of zinc and oxygen. A small difference can also be observed between absorption bands of Zn-O and a slight shift to a lower wave number due to a change in the lattice parameters of the ZnO nanoparticles (Khorsand-Zak *et al*. 2011). In addition, the peaks at 3337 cm^{-1} and 1377 cm^{-1} corresponding to stretching and bending vibrations of the hydroxyl groups, respectively and the peaks at around 1050 cm^{-1} attributed to the pyranose ring ether band of CNC (Mo *et al.* 2009) in ZnO/CNC nanocomposites showed a shift to higher wavenumbers and became wider due to a strong interaction between the oxygen atoms of CNC and ZnO particles. Comparison of these bands for samples 1, 2, and 3 indicates some differences in their shape; this can be explained by the significant differences in the interaction between the two components of the nano-composites.

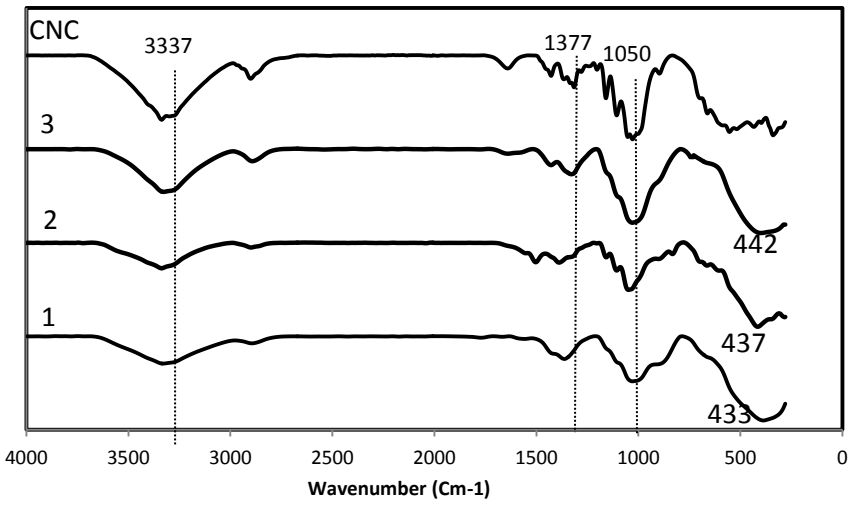

Fig. 1. FTIR spectra of ZnO/CNC nanocomposites (samples 1, 2, and 3) and CNC

Figure 2 (a, b, and c) displays TEM micrographs of the samples 1, 2, and 3, respectively. The grey network background corresponds to CNC, and the black spots are the ZnO nanoparticles.

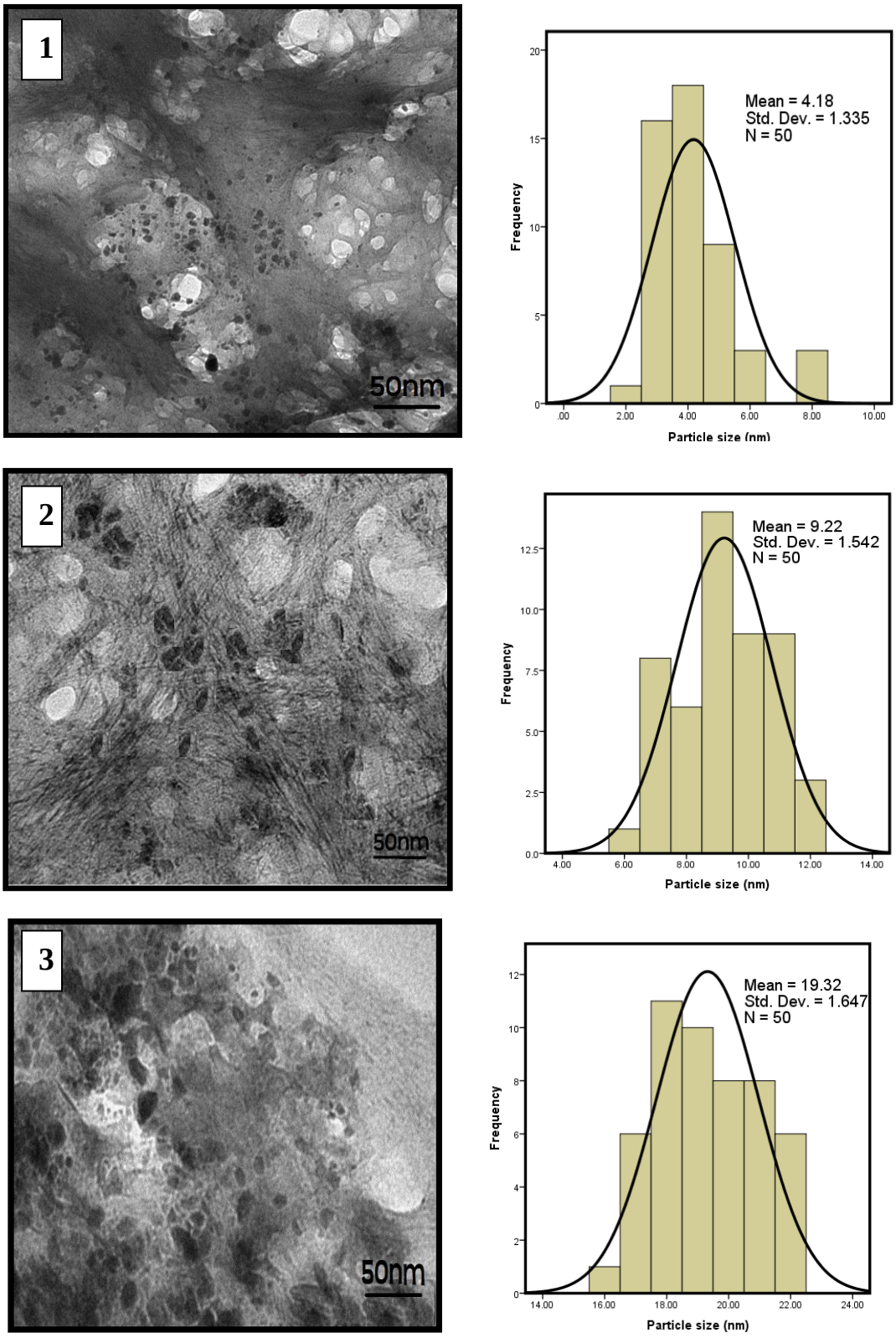

Fig. 2. TEM images and histograms of ZnO/CNC nanocomposites samples 1, 2, and 3

The results show hexagonal shapes with smooth surfaces dispersed within the CNC that have an average size of 4.18, 9.22, and 19.32 nm for samples 1, 2, and 3, respectively. It was found that by increasing the molar ratio of ZnO to CNC, the average size increased and the dispersion of particles decreased. Considering the TEM images, sample 1 was selected as the best ratio, based on the small particle size and good dispersion of nanoparticles.

Figure 3 shows the XRD spectra of the synthesized ZnO/CNC nanocomposites. Positions and intensities of all relative peaks of the ZnO nanoparticles matched the Joint Committee on Powder Diffraction Standard (JCPDS) card number 36-1451. All the recorded peak intensity profiles were characteristic of nanoparticles' hexagonal wurtzite structure. Although the position of the different ZnO peaks were similar for all samples, the width of peaks decreased and the intensity of peaks increased gradually as the content of ZnO increased, indicating increased crystal size and crystallinity (Wang and Xie 2008). It can be seen that the reflection peaks clearly became broader in sample 1, indicating a reduction in crystallite size of particles. All peaks corresponding to the CNC are also observable in samples 1 to 3. However, it was found that the signals intensity due to the 200 and 220 planes in samples 1 and 2 were quite low and hardly observable. This may be a result of insufficient ZnO/CNC powder coating on the glass slide, which caused difficulty in detection of the crystal plane. The mean particle sizes of the samples were evaluated from FWHM using Scherrer's equation (Shen *et al.* 2006),

$$d = 0.89\lambda/ß\cos\Theta \quad (1)$$

where d, λ, Θ, and $ß$ indicate the mean particle size, the X-ray wavelength (1.5406A°), Bragg diffraction angle corresponding to the (1 0 1) plane, and full width at half maximum (FWHM) of the (1 0 1) plane, respectively. The average particle size for the ZnO nanoparticles was 4.8, 11.4, and 20.5 nm for samples 1, 2, and 3, respectively. These values are close to the obtained particle size from the TEM images.

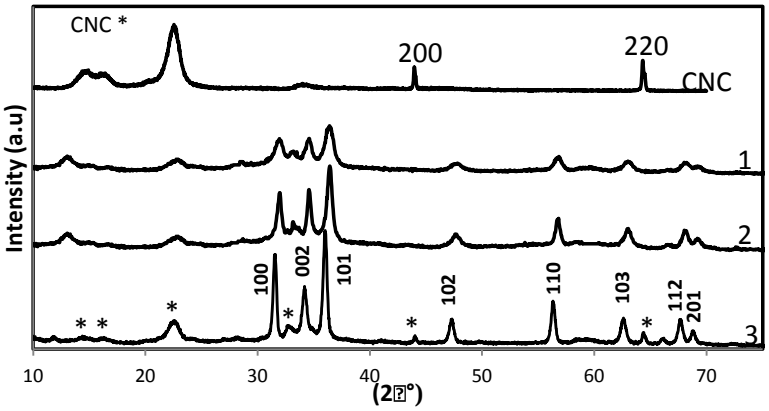

Fig. 3. XRD Spectra of ZnO/CNC nanocomposites (samples 1, 2, and 3)

The UV-vis absorption spectra of aqueous suspensions of the ZnO/CNC nanocomposites are shown in Fig. 4a. The exciton absorption peaks of the samples were in a range of 346 to 357 nm. These peaks can be assigned to the basic band gap absorption of ZnO because the electron transitions from the valence band to the conduction band ($O2p \rightarrow Zn3d$) (Khorsand-Zak *et al.* 2011). In addition, a blue shift was

seen for products that could be due to changes in the morphologies, size, and surface microstructures of particles. Furthermore, the direct band gaps of samples estimated from a plot of $(\alpha hv)^2$ versus the photo energy (hv) consistent with the Kubelka-Munk model (Yu *et al.* 2008), shown in Figure 4b, were 3.40 eV, 3.32 eV, and 3.27 eV for samples 1, 2, and 3, respectively. Such an increase in the ZnO band gap energy is in good agreement with the corresponding blue shift observed in the UV absorption edge.

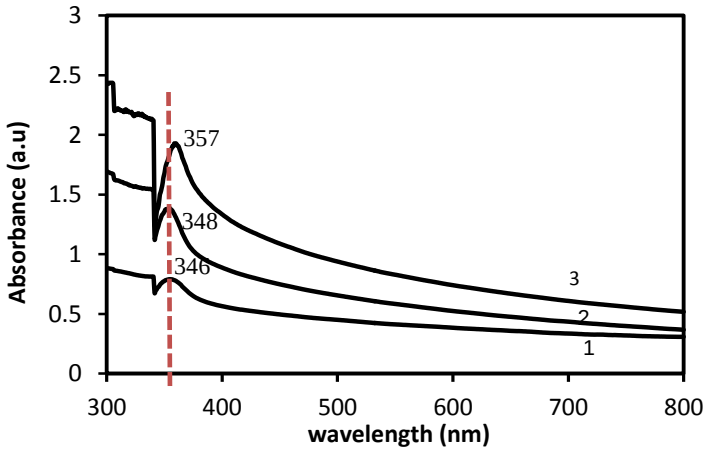

Fig. 4a. UV Spectroscopy of ZnO/CNC nanocomposites

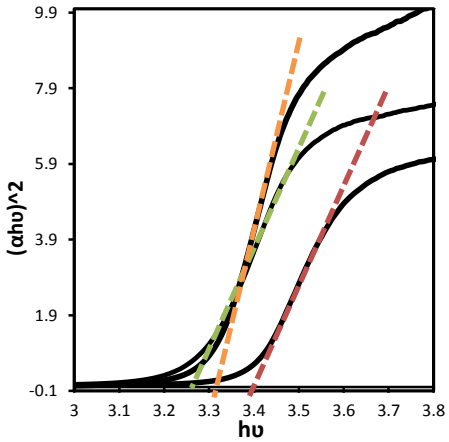

Fig. 4b. Plots of $(\alpha h\upsilon)^2$ versus hυ of ZnO/CNC nanocomposites

Thermogravimetric analysis was carried out in order to determine the effect of the synthesized ZnO nanoparticles on the thermal properties of the cellulose nanocrystals. Figure 5 shows the TG curves of the cellulose nanocrystals and the ZnO/CNC nanocomposites. The thermal decomposition of the cellulose nanocrystals includes depolymerisation, dehydration, and decomposition of glycosyl units, followed by the formation of a charred residue (Araki *et al.* 1998). The two main steps observed in the nanocomposites correspond to the thermal degradation of the CNC (Dahiya and Rana 2004). The thermal analysis demonstrated that thermal decomposition of the cellulose nanocrystals was initiated at 138 °C, with 20.43 wt% residue at the end of degradation. The onsets of thermal degradation for the ZnO/CNC nanocomposites were found at 230, 223, and

215 °C with 47.39, 65.48, and 76.90 wt% residue for samples 1, 2, and 3, respectively. The cellulose nanocrystals in the ZnO/CNC nanocomposites exhibited better thermal stability compared to the original cellulose nanocrystal. The improvement can be ascribed to the interaction between the ZnO and the CNC, which was more considerable for the smaller-sized ZnO nanoparticles with greater surface area. The amount of ZnO nanoparticles was estimated by comparing the percentage residue of the ZnO/CNC nanocomposites and the CNC at the end of degradation. The content of ZnO was estimated to be about 26.96, 45.05, and 56.47 wt% for samples 1, 2, and 3, respectively.

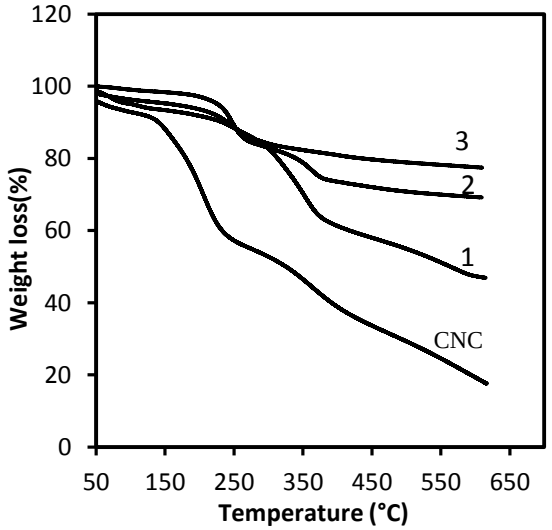

Fig. 5. TG Thermograms of CNC and ZnO/CNC nanocomposites

Table 1. Inhibition Zone of ZnO/CNC Nanocomposites Against *Staphylococcus aureus* and *Salmonella choleraesuis* Bacteria

Sample	Diameter of zone (mm)	Diameter of zone (mm)
	Staphylococcus aureus	*Salmonella choleraesuis*
1	14	10
2	12	9
3	9	7
ZnO	5	5

The antibacterial ability of the ZnO/CNC nanocomposites was determined in terms of the inhibition zone created on agar around the paper discs. The average diameters of the inhibition zones of all samples against *Staphylococcus aureus* and *Salmonella choleraesuis* are shown in Table 1. It is evident that the antibacterial activity of the samples was stronger against Gram-positive *Staphylococcus aureus* than Gram-negative *Salmonella choleraesuis*. Stronger antibacterial activity against Gram-positive bacteria has also been previously reported (Lu *et al.* 2008; Yang *et al.* 2006; Fang *et al.* 2006). The cell wall of Gram-negative bacteria has an outer lipopolysaccherice (LPS) membrane that protects the peptidoglycan layer. In addition, it helps bacteria to survive in environments where external materials exist that can harm it. On the other hand, the antibacterial activity of the samples increases by decreasing the size of particles. The greatest antibacterial ability was obtained from sample 1 with an average particle size of 4.18 nm. In this study, ZnO nanoparticles (20 nm) without CNC showed less powerful

effect against Gram-positive and negative bacteria in comparison to sample 3. Our results which are in favor of ZnO/CNC could be the outcome of a tight attaching of cellulose nanocrystals to the bacterial cover. This study proves which cellulose nanocrystals can be used to prepare colloidal suspensions with strong antibacterial effect.

CONCLUSIONS

1. ZnO nanoparticles with a hexagonal wurtzite structure and average size of less than 20 nm were successfully synthesized in the CNC using a sol-gel method.
2. The best composition of the ZnO/CNC nanocomposite was selected based on its small size and good dispersion of particles in the CNC, which showed good antibacterial activity and the best thermal properties.
3. The band gap of the ZnO nanoparticles was estimated from the UV-vis absorption. There was a blue shift in the absorption edge after decreasing the size of the ZnO nanoparticles.
4. The antibacterial studies showed that the ZnO/CNC nanocomposites are stronger antibacterial materials against Gram-positive *Staphylococcus aureus* than Gram-Negative *Salmonella choleraesuis* bacteria, and CNC can provide strong anti-microbial power for ZnO nanoparticles.

ACKNOWLEDGMENTS

The researchers would like to express their thanks to all those who assisted during the experiments and gathering of the data.

REFERENCES CITED

Amornpitoksuk, P., Suwanboon, S., Sangkanu, S., Sukhoom, A., Wudtipan, J., Srijan, K., and Kaewtaro, S. (2011). "Synthesis, photocatalytic and antibacterial activities of ZnO particles modified by diblock copolymer," *Powd. Technol.* 212, 432-438.

Araki, J., Wada, M., Kuga, S., and Okano, T. (1998). "Flow properties of microcrystalline cellulose suspension prepared by acid treatment of native cellulose," *Colloids Surf. A* 42(1), 75-82.

Beck-Candanedo, S., Roman, M, and Gray, D. G. (2005). "Effect of reaction conditions on the properties and behavior of wood cellulose nanocrystal suspensions," *Biomacromol.* 6(2), 1048-1054.

Cai, S., Kimura, J., Wada, M., and Kuga, S. (2009). "Nanoporous cellulose as metal nanoparticles support," *Biomacromol.* 10, 87-94.

Chronakis, I. S. (2005). "Novel nanocomposites and nanoceramics based on polymer nanofibers using electrospinning process- A review," *J. Mater. Process Technol.* 167(2-3), 283-293.

Dahiya, J. B., and Rana, S. (2004). "Thermal degradation and morphological studies on cotton cellulose modified with various arylphosphorodichloridites," *Polym. Int.* 53, 995-1002.

De Souza Lima, M. M., Wong, J. T., Paillet, M., Borsali, R., and Pecora, R. (2003). "Translational and rotational dynamics of rodlike cellulose whiskers," *Langmuir* 19, 24-29.

Fang, M., Chen, J. H., Xu, X. L., Yang, P. H., and Hildebrand, H. F. (2006). "Antibacterial activities of inorganic agents on six bacteria associated with oral infections by two susceptibility tests," *Int. J. Antimicrob. Agents* 27, 513-517.

Galoppini, E., Rochford, J., Chen, H., Saraf, G., Lu, Y., Hagfeldt, A., and Boschloo, G. (2006). "Fast electron transport in metal organic vapor deposition grown dye-sensitized ZnO nanorod solar cells," *J. Phys. Chem. B* 110(33), 16159-16161.

He, J. H., Kunitake, T., and Nakao, A. (2003). "Facile in situ synthesis of noble metal nanoparticles in porous cellulose fibers," *Chem. Mater*. 15, 4401-4406.

Height, M. J., Pratsinis, S. E., Mekasuwandumrong, O., and Praserthdam, P. (2006). "Ag-ZnO catalysts for UV-photodegradation of methylene blue," *Appl. Catal. B: Environ.* 63(3-4), 305-312.

Hong, R. Y., Li, J. H., Chen, L. L., Liu, D. Q., Li, H. Z., and Zheng, Y. (2009). "Synthesis, surface modification and photocatalytic property of ZnO nanoparticles," *J. Ding. Powd. Technol*. 189, 426-432.

Huang, M. H., Mao, S., Feick, H., Yan, H., Wu, Y., Kind, H., Weber, E., Russo, R., and Yang, P. (2001). "Room-temperature ultraviolet nanowire nanolasers," *Science* 292(5523), 1897-1899.

Khorsand Zak, A., Ebrahimizadeh Abrishami, M., Abd. Majid, W. H., Yousefi, R., and Hosseini, S. M. (2011). "Effects of annealing temperature on some structural and optical properties of ZnO nanoparticles prepared by a modified sol–gel combustion method," *Ceram. Internat.* 37, 393-398.

Liu, H., Wang, D., Shang, S., and Song, Z. (2010). "Synthesis and characterization of Ag–Pd alloy nanoparticles/carboxylated cellulose nanocrystals nanocomposites," *Carb. Polym*. 83, 38-43.

Liu, H., Wang, D., Song, Z., and Shang, S. (2011). "Preparation of silver nanoparticles on cellulose nanocrystals and the application in electrochemical detection of DNA hybridization," *Cellulose* 18, 67-74.

Liu, R. L., Ye, S. H., Xiong, X. P., and Liu, H. Q. (2010). "Fabrication of TiO_2/ZnO composite nanofibers by electrospinning and their photocatalytic property," *Mater. Chem. Phys*. 121, 432-439.

Liu, R. L., Huang, Y. X., Xiao, A. H, and Liu, H. Q. (2010). "Preparation and photocatalytic property of mesoporous ZnO/SnO_2 composite nanofibers," *J. Alloys Comp*. 503, 103-110.

Lu, W., Liu, G., Gao, S., Xing, S, and Wang, J. (2008). "Tyrosine-assisted preparation of Ag/ZnO nanocomposites with enhanced photocatalytic performance and synergistic antibacterial activities," *Nanotech.* 19, 1-10.

Mo, Z.-L., Zhao, Z.-L., Chen, H., Niu, G.-P., and Shi, H.-F. (2009). "Heterogeneous preparation of cellulose-polyaniline conductive composites with cellulose activated by acids and its electrical properties," *Carbo. Polym.* 75(4), 660-664.

Nishino, T., Matsuda, I., and Hirao, K. (2004). "All-cellulose composite," *Macromolecules* 37(20), 7683-7687.

Patel, A. C., Li, S. X., Wang, C., Zhang, W. J., and Wei, Y. (2007). "Electrospinning of porous silica nanofibers containing silver nanoparticles for catalytic applications," *Chem. Mater.* 19, 1231-1238.

Shen, L. M., Bao, N. Z., and Yanagisawa, K. (2006). "Direct synthesis of ZnO nanoparticles by a solution-free mechanochemical reaction," *Nanotechnology,* 17, 5117-5123.

Shin, Y., Bae, I., Arey, B. W., and Exarhos, G. J. J. (2008). "Facile stabilization of gold-silver alloy nanoparticles on cellulose nanocrystal," *Phys. Chem. C* 112, 4844-4848.

Stoimenov, P. K., Klinger, R. L., Marchin, G. L., and Klabunde, K. J. (2002). "Metal oxide nanoparticles as bactericidal agents," *Langmuir* 18, 6679-6686.

Sturcova, A., Davies, G. R., and Eichhorn, S. J. (2005). "Elastic modulus and stress-transfer properties of tunicate cellulose whiskers," *Biomacromol.* 6, 1055-1061.

Tam, K. H., Djurisic, A. B., Chan, C. M. N., Xi, Y. Y., Tse, C. W., Leung, Y. H., Chan, W. K., Leung, F. C. C., and Au, D. W. T. (2008). "Antibacterial activity of ZnO nanorods prepared by hydrothermal method," *Thin Solid Films* 516, 6167-6174.

Wang, H., and Xie, C. (2008). "Effect of annealing temperature on the microstructures and photocatalytic property of colloidal ZnO nanoparticles," *J. Phys. Chem. Solids* 69, 2440-2444.

Wang, M., Hsieh, A. J., and Rutledge, G. C. (2005). "Electrospinning of poly(MMA-co-MAA) copolymers and their layered silicate nanocomposites for improved thermal properties," *Polymer* 46(10), 3407-3418.

Yang, L., Mao, J., Zhang, X., Xue, T., Hou, T., Wang, L., and Tu, M. (2006). "Preparation and characteristics of Ag/nano-ZnO composite antimicrobial agent," *Nanosci.* 11, 44-48.

Yin, Z. Y., Sun, S., Salim, T., Wu, S. X., Huang, X., He, Q.Y., Lam, Y. M., and Zhang, H. (2010). "Organic photovoltaic devices using highly flexible reduced graphene oxide films as transparent electrodes," *ACS Nano.* 4, 5263-5268.

Yu, J., Li, C., and Liu. S. (2008). "Effect of PSS on morphology and optical properties of ZnO," *J. Colloid Interface Sci.* 326, 433-438.

Zhang, L., Ding, Y., Povey, M., and York, D. (2008). "ZnO nanofluids- A potential antibacterial agent," *Prog. Nat. Sci.* 18, 939-944.

Zhang, Q., Zhang, S., Xie, C., Zeng, D., Fan, C., Li, D., and Bai, Z. (2006). "Characterization of Chinese vinegars by electronic nose," *Sens. Actuators B* 119, 538-546.

Article submitted: October 17, 2012; Peer review completed: February 6, 2012; Revised version received: February 13, 2013; Accepted: February 17, 2013; Published: February 21, 2013.